Hindawi
Adsorption Science & Technology
Volume 2022, Article ID 7582756, 13 pages
https://doi.org/10.1155/2022/7582756

Research Article

Adsorption of Pb(II) from Water onto ZnO, TiO_2, and Al_2O_3: Process Study, Adsorption Behaviour, and Thermodynamics

Nagwan G. Mostafa, Ahmad F. Yunnus, and Abdelsalam Elawwad

Environmental Engineering Department, Faculty of Engineering, Cairo University, El-Gamaa St., 12613 Giza, Egypt

Correspondence should be addressed to Abdelsalam Elawwad; elawwad@cu.edu.eg

Received 20 November 2021; Accepted 15 January 2022; Published 27 January 2022

Academic Editor: George Kyzas

This study is aimed at comparing the use of zinc oxide (ZnO), titanium dioxide (TiO_2), and aluminium oxide (Al_2O_3) for removing lead ions from water through adsorption. The point of zero charge was obtained for ZnO, TiO_2, and Al_2O_3 and was found to be 7.3, 7.1, and 9.0, respectively. The effect of pH, adsorbent dose, contact time, initial concentrations, and temperature was investigated in batch experiments. The optimal conditions obtained were 7, 2 g/L, 120 mins, 100 ppm, and 41°C, respectively, where the optimal removal efficiencies were 98.43%, 96.45%, and 85.50% for ZnO, TiO_2, and Al_2O_3, respectively. In addition, analyses of adsorption kinetics, mechanisms, isotherms, and thermodynamics were performed. The adsorption kinetics of Pb(II) were compared to popular models, and it was found that the pseudo-second-order (PSO) model best fitted the Pb(II) uptake for all adsorbents at correlation coefficient ($R^2 \geq 0.96$). The adsorption isotherms of Pb(II) were also compared to popular models, and it was found that the Pb(II) uptake by TiO_2 and ZnO was well-described by the Langmuir model ($R^2 \geq 0.96$) with maximum adsorption capacities of 55.04 and 58.88 mg/g, respectively. On the other hand, the behaviour of Al_2O_3 is described more accurately by the Dubinin-Radushkevich (D-R) model ($R^2 = 0.96$), and the maximum adsorption capacity was 53.64 mg/g. The isotherm analysis proved that the limiting step of the adsorption process is the film diffusion mechanism. In addition, studying the heat of adsorption of Pb(II) implied that the adsorption is endothermic due to the positive values of enthalpy ($\Delta H^\circ \geq 30$) for all adsorbents. The absorbents were characterized using scanning electron microscopy (SEM) and energy-dispersive X-ray spectroscopy (EDX) to study the morphology of surfaces and the chemical characterization of the adsorbents to ensure that adsorption is achieved. ZnO showed better performance for the uptake of lead followed by TiO_2 then Al_2O_3.

1. Introduction

Contamination of aquatic environments by heavy metals is one of the most major environmental challenges because of their flexibility, aggregation, persistence, and nonbiodegradable nature. Some of the toxic heavy metals, in particular lead, can have severe and poisonous effects on human beings and marine organisms even at trace levels [1, 2]. This problem is exacerbated in developing countries, where polluting industries are rapidly developed for various applications, such as mining operations, tanneries, batteries, fertilizer, pesticides, paper industries, and coke factories [3].

Various adsorbents are used to remove heavy metals, such as arsenic, cadmium, nickel, mercury, chromium, zinc, and lead, from aqueous solutions. These adsorbents include carbon-based adsorbents [4], bioadsorbents [5], low-cost adsorbents [6], and polymeric nanosorbents [7]. This study sheds light on lead, which is one of the most toxic heavy metals that attracts considerable attention from environmentalists. Lead is discharged into aquatic ecosystems from various industrial activities, such as storage batteries, ceramic glass industries, mining, plating, coating, and automotive industries. Another potential source for lead contamination is the wide utilization of agricultural chemicals such as fertilizers and fungicidal sprays [8]. In addition to the pollution of aquatic environments, the adverse effects of lead on human health have been well documented and characterized. Lead poisoning causes serious harm to the kidneys,

damages the central nervous system and liver, and can result in cancer and brain damage, in addition to abnormalities in living creatures' organs [9, 10].

In response to this, several techniques have been developed to remove harmful heavy metals from aqueous solutions and maintain environmental safety, such as chemical precipitation, ion exchange, membrane separation, adsorption, and electrochemical removal [11]. Among these techniques, adsorption has recently gained growing importance for being an efficient, effective, and economical technique. It provides high quality treated outputs, low operating cost, high design and operating flexibility, and high removal efficiency in the absence of interference of any competing additives [12].

A wide range of adsorbents was used to extract lead, such as activated carbon [13], modified alginate aerogel with melamine/chitosan [11], reduced graphene oxide-Fe_3O_4 [8], and pea peel waste [14]. The use of zinc oxide (ZnO), titanium dioxide (TiO_2), and aluminium oxide (Al_2O_3) as adsorbents for removal of different constituents from wastewater is promising in light of its advantages, such as availability, simplicity, nontoxic nature, resilience to corrosive elements, and a strong affinity for metal ions used in wastewater treatment [15]. Efficient removal of heavy metals was reported in the literature using ZnO nanocomposites and nanoparticles [16, 17], TiO_2 composites and nanoparticles [2, 18], and Al_2O_3 nanocomposites and nanoparticles [19–22]. However, few studies compared the capacities of these three adsorbents in the removal of heavy metals.

Despite the studies mentioned above, limited studies compared the adsorption capacity and removal mechanism for lead adsorption onto zinc oxide (ZnO), titanium dioxide (TiO_2), and aluminium oxide (Al_2O_3) under the same conditions. To our knowledge, no study compared the thermodynamics of these metal oxides for this particular case. Thus, this research is aimed at studying and comparing the use of these metal oxides for lead removal from water by adsorption. The effect of pH, adsorbent doses, contact time, initial concentrations, and temperature on lead removal was investigated. The experimental results were analyzed using pseudo-first order (PFO), pseudo-second order (PSO), Elovich equation, the intraparticle diffusion model, and the Boyd kinetic models to determine the most compatible adsorption kinetic and mechanism model. Subsequently, the equilibrium data were investigated using various isotherm models, such as Langmuir, Freundlich, Temkin, and Dubinin-Radushkevich (D-R) models, to determine the appropriate isotherms for the characterization of the behaviour of lead adsorption on metal oxides.

2. Materials and Methods

Lead nitrate (Pb $(NO_3)_2$), manufactured by Loba Chemie Pvt. Ltd., India, 99% extra pure, was used to prepare the contaminated solution. A 1000 ppm stock solution is prepared by dissolving 1.58 g of lead nitrate in 1000 mL of deionized water containing 10% (*v*/*v*) of hydrochloric acid (HCl) for 24 h to prevent the precipitation of Pb(II) due to hydrolysis. Other standard solutions were prepared by diluting this solution as required to acquire working solutions between 50 and 150 mg/L of Pb(II). The initial pH of any experimental solutions was modified by adding HCl or sodium hydroxide (NaOH) solutions.

Zinc oxide 99% pure (AR zinc white), titanium dioxide, 98% extra pure, and aluminium oxide active (basic), manufactured by Loba Chemie Pvt. Ltd., India, were used as adsorbents. The surface of materials before and after adsorption was studied using scanning electron microscopy (SEM) and energy-dispersive X-ray spectroscopy (EDX). By following procedures described in earlier studies [23, 24], the points of zero charge for each of the three adsorbents using the pH drift method were found to be 7.3, 7.1, and 9.0 for ZnO, TiO_2, and Al_2O_3, respectively, see Figure 1.

The adsorption experiments are divided into several batches, where each batch evaluates a specific parameter that affects the adsorption process and determines its optimal value among the tested range. The tested parameters were pH of the solution, adsorbent dose, contact time, initial concentration of Pb(II), and temperature. The effect of pH was investigated by adjusting the solution pH between pH 3 and 9 using 0.1 M of nitric acid (HNO_3) and NaOH. The adsorbent dosage tested range varied between 0.01 and 0.05 g. The effect of contact time was investigated by varying the contact time from 5 to 120 min. The impact of the initial concentration of lead was studied between 50 and 150 ppm, and the temperature effect was studied between 18 and 41°C. For each batch, the solution flasks were shaken to ensure that the solution reached equilibrium (maximum adsorption capacity). At the end of each batch, the solution was centrifuged, filtered using a filter paper (Whitman number 45), and analyzed using inductively coupled plasma (ICP) spectrometry (model Ultima 2 JY Plasma) to measure the final concentration of lead in water samples complies to Environmental Protection Agency (EPA-US) measurement technique [25]. The adsorption percentage and the capacity of adsorption can be calculated according to Equation (1) and Equation (2), respectively, [26]:

$$\text{Adsorption percentage\%} = \frac{C_o - C_e}{C_o} \times 100, \tag{1}$$

$$q_e = \frac{(C_o - C_e)}{m} \times V, \tag{2}$$

where q_e is the mass of metal ions adsorbed per unit weight of the adsorbent at equilibrium (mg adsorbate/g adsorbent), C_0 is the initial concentration of the metal ions (mg/L), C_e is the equilibrium concentration of the metal ion (mg/L), V is the volume of the metal ion solution (mL), and m is the mass of the adsorbent (mg).

3. Results and Discussion

3.1. Adsorption Studies

3.1.1. Effect of pH Solution. The effect of the initial pH of the solution on the percentage of Pb(II) removed by adsorption was investigated at four different pH values, namely, 3, 5, 7,

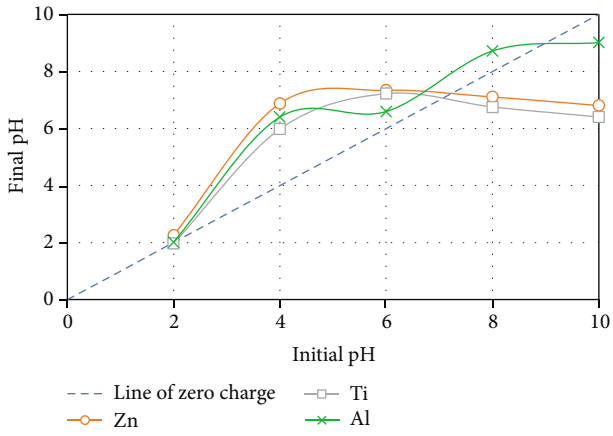

Figure 1: pH drift method for all adsorbents.

and 9, using an initial adsorbent mass of 0.02 g with 25 mL of contaminated solution. The initial Pb(II) concentration was 100 ppm at room temperature 29 ± 1°C. The mixture was shaken for 120 min at a constant stirring velocity of 150 rpm. The final Pb(II) concentration values were measured, and the adsorption percentage was calculated using Equation (1). The optimal removal efficiencies were 94.66%, 87.97%, and 65.34% for ZnO, TiO_2, and Al_2O_3, respectively, at a pH value of 7.0 as shown in Figure 2(a). The adsorption percentage increased as the initial pH of the solution increased from pH 3.0 to 7.0 for all adsorbents used. The surface of the adsorbents became more negatively charged, and subsequently, the electrostatic attraction (ion exchange) between the metal ions and surface of the adsorbents probably increased. The increase in adsorption percentage may be attributed to the interaction of Pb^{2+}, $Pb(OH)^+$, and $Pb(OH)_2$ with the functional groups present on the surface of the adsorbents due to ion exchange mechanism or by hydrogen bonding [27] as shown in Figure 3 and the following reactions:

Ion exchange mechanism:

$$\begin{aligned} 2(-ROH) + Pb^{2+} &\longrightarrow 2(RO)Pb + 2H^+ \\ -ROH + Pb(OH)^+ &\longrightarrow (-RO)\,Pb(OH) + H^+ \end{aligned} \quad (3)$$

Hydrogen bonding:

$$2(-ROH) + Pb\,(OH)_2 \longrightarrow (-ROH)_2 + Pb(OH)_2 \quad (4)$$

At higher pH values (7.0–9.0), a decrease in the adsorption percentage was observed in ZnO and TiO_2 due to the formation of soluble hydroxyl complexes. However, for Al_2O_3, an increase in adsorption percentage was observed since the value of pH at the point of zero charge (pH_{PZC}) for Al_2O_3 is 9.0, see Figure 1. As the pH of the solution increases, the adsorbent surface becomes less positively charged which allows for more adsorption of Pb(II) cations. For the following batches, an optimal pH value of 7.0 is used. Below this optimal value, competition between Pb(II) ions and H_3O^+ reduces the adsorption efficiency, while higher pH values result in hydrolysis of lead species which encourages precipitation and prevents quantitative adsorption.

3.1.2. Effect of Adsorbent Dosage. This batch of experiments was conducted with different concentrations of adsorbents, namely, 0.01, 0.02, 0.03, 0.04, and 0.05 g, at the optimal initial pH value, with 25 mL of the contaminated solution. The initial Pb(II) concentration was 100 ppm at room temperature of 29 ± 1°C, and the blend was shaken for 120 min at a constant stirring velocity of 150 rpm. The final Pb(II) concentration values were measured, and the adsorption percentage was calculated using Equation (1). The maximum removal efficiencies achieved were 95.27%, 90.46%, and 70.8% for ZnO, TiO_2, and Al_2O_3, respectively, at a corresponding adsorbent dosage of 0.05 g as shown in Figure 3(b). The adsorption percentage increases as the doses of the adsorbents in the solution increase from 0.01 to 0.05 g for all adsorbents used. These results can be interpreted as increasing the adsorbent dose from 0.01 to 0.05 g provides more active binding sites for the adsorption process. Thus, more Pb(II) ions are adsorbed onto the surface of the adsorbent since the competition between molecules for active binding sites is reduced. The optimal dose obtained was 0.05 g, applied for the subsequent batches.

3.1.3. Effect of Contact Time. This batch of experiments was conducted at different contact times, namely, 15, 30, 60, 90, and 120 min, with optimal pH value and adsorbent dose of 7.0 and 0.05 g, respectively, at room temperature of 29 ± 1 °C and 25 mL of contaminated solution. The initial Pb(II) concentration was 100 ppm at a constant stirring velocity of 150 rpm. The final Pb(II) concentration values were measured, and the adsorption percentage was calculated using Equation (1). The maximum removal efficiencies obtained were 96.17%, 91.75%, and 79.5% for ZnO, TiO_2, and Al_2O_3, respectively, at a contact time of 120 min as illustrated in Figure 2(c). The adsorption percentage increases as the process contact time increases from 15 to 120 min for all the adsorbents used. However, it appears that the rate of lead uptake is the greatest within the initial 15 min because of the availability of active binding sites on the surface of the adsorbents. Consequently, it can be seen that the equilibrium of lead uptake by all the adsorbents is reached within 90 min, following which there is an insignificant change in lead uptake until 120 min.

3.1.4. Effect of Initial Concentration of Pb(II). This batch was conducted at different initial concentrations of Pb(II), namely, 50, 75, 100, 125, and 150 ppm, at the optimal pH value and the optimal adsorbent dose obtained from previous batches with 25 mL of contaminated solution at room temperature of 29 ± 1°C. The blend was shaken for 120 min at a constant stirring velocity of 150 rpm. The final Pb(II) concentration values obtained were measured, and the adsorption percentage was calculated using Equation (1). The maximum removal efficiencies were 96.17%, 91.75%, and 79.50% for ZnO, TiO_2, and Al_2O_3, respectively, at an initial concentration of 100 ppm for all adsorbents as shown in Figure 2(d). The results suggest that the percentage of

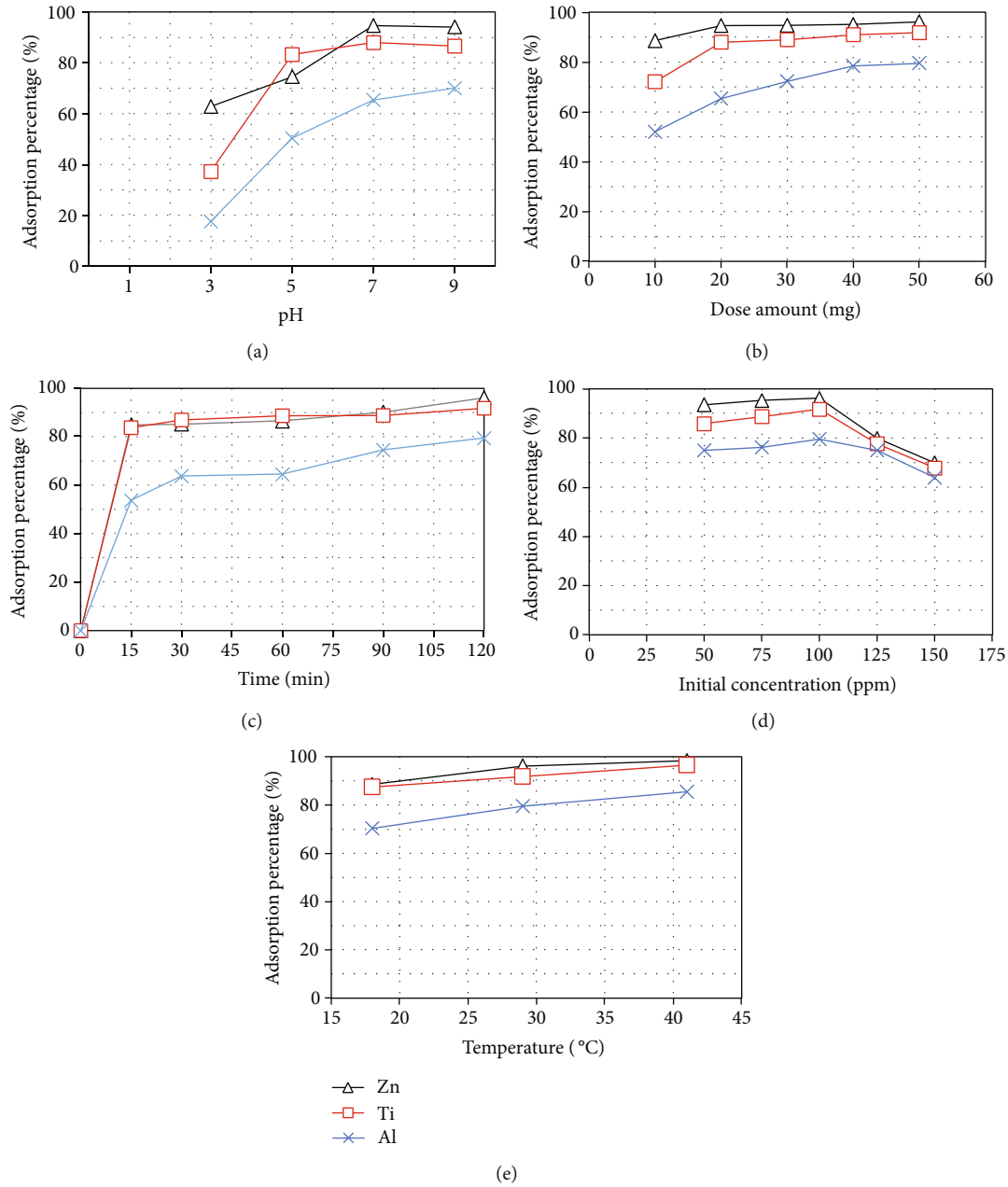

Figure 2: Effect of different parameters on the adsorption of Pb(II) onto all adsorbents: (a) initial pH of the solution, (b) adsorbent dosage, (c) contact time, (d) initial concentration of Pb(II), and (e) temperature.

Pb(II) removal by adsorption increases as the initial Pb(II) concentration increases to a certain extent. The adsorption percentage increased from 93.55 to 96.17% for ZnO, from 85.88 to 91.75% for TiO_2, and from 61.50 to 79.50% for Al_2O_3 as the initial concentration of Pb(II) is increased from 1 to 100 ppm. Thereafter, the percentage of Pb(II) removal decreases as the initial Pb(II) concentration increases to a value of 150 ppm. This can be interpreted as at a fixed amount of adsorbent; the high initial Pb(II) concentration leads to an excess amount of available particles compared with the active binding site on the adsorbent surface, so that the percentage of Pb(II) removal by adsorption decreases.

3.1.5. Effect of Temperature. This batch was conducted at different temperature values, namely, 18, 29, and 41°C, at an optimal pH of 7.0, an optimal dose of adsorbents equal to 0.05 g, and a 25 mL contaminated solution of 100 ppm Pb(II) as an optimal initial concentration. The blend was shaken for 120 min at a constant stirring velocity of 150 rpm. The final Pb(II) concentration values were measured, and the adsorption percentage was calculated using Equation (1). The maximum removal efficiencies were 98.43%, 96.45%, and 85.50% for ZnO, TiO_2, and Al_2O_3, respectively, at a temperature of 41°C for all adsorbents as shown in Figure 2(e).

The results showed that the percentage of Pb(II) removal by adsorption increases as the temperature increases. The

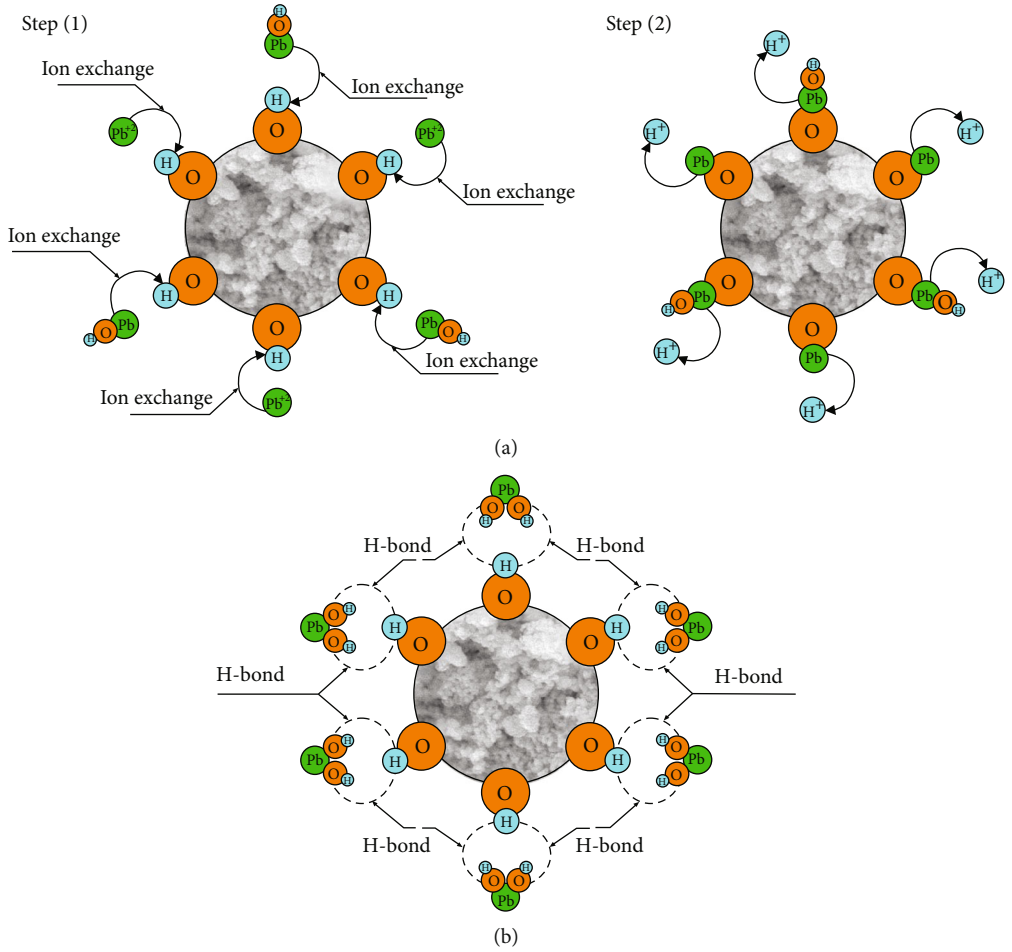

FIGURE 3: Adsorption mechanisms of Pb(II) on metals adsorbent surfaces: (a) ion exchange mechanism and (b) hydrogen bonding mechanism.

adsorption percentage was observed to increase from 88.55 to 98.43% for ZnO, from 87.46 to 96.45% for TiO_2, and from 70.34 to 85.48% for Al_2O_3 as the temperature was increased from 18 to 41°C. This indicates that the adsorption process is an endothermic reaction for all adsorbents.

3.2. Kinetic Studies. The uptake rate of Pb(II) ions from the water can be predicted by adsorption kinetics. Three mathematical models, namely, pseudo-first order (PFO), pseudo-second order (PSO), and Elovich equation, were used to fit the uptake rate using the Pb(II) adsorption data at different contact times. The PFO model, PSO model, and Elovich equation are expressed by Equations (5), (6), and (7), respectively [28–30].

$$\mathrm{Log}(q_e - q_t) = \mathrm{Log}q_e - \frac{k_1}{2.303}t, \tag{5}$$

$$\frac{t}{q_t} = \frac{1}{k_2 q_e^2} + \frac{1}{q_e}t, \tag{6}$$

$$q_t = \frac{1}{b}\ln(ab) + \frac{1}{b}\ln(t), \tag{7}$$

where q_e is the mass of absorbed pollutant per unit weight of adsorbent at equilibrium (mg/g), q_t is the adsorbed amount of adsorbent at time t (mg/g), k_1 is the PFO equation constant (min^{-1}), t is time (min), k_2 is the rate constant of PSO equation (g/mg·min), a is a parameter that describes the initial rate of adsorption (mg/g·min), and $1/b$ is a parameter relative to the number of adsorption sites on the surface of the adsorbents (mg/g).

The PSO model's correlation coefficient (R^2) compared to the adsorption results was greater than that of the PFO model and Elovich equation, which suggests that the PSO model best describes the kinetics of the adsorption process. This also indicated that chemisorption was the reaction's rate-limiting part, as shown in Figures 4(a)–4(c). The kinetic parameters of these models are summarized in Table 1.

3.3. Adsorption Mechanisms. The adsorption process consists of three controlling steps: (1) the motion of the adsorbate from the bulk liquid to the surrounding film of the adsorbent, a process known as *film diffusion*, (2) the transport of the adsorbate from the film to the adsorbent surface, a process known as *surface adsorption*, and (3) the transmission of the adsorbate to the internal active sites, a process known as *intraparticle diffusion* [31]. The active sites sequentially attach to these metal ions.

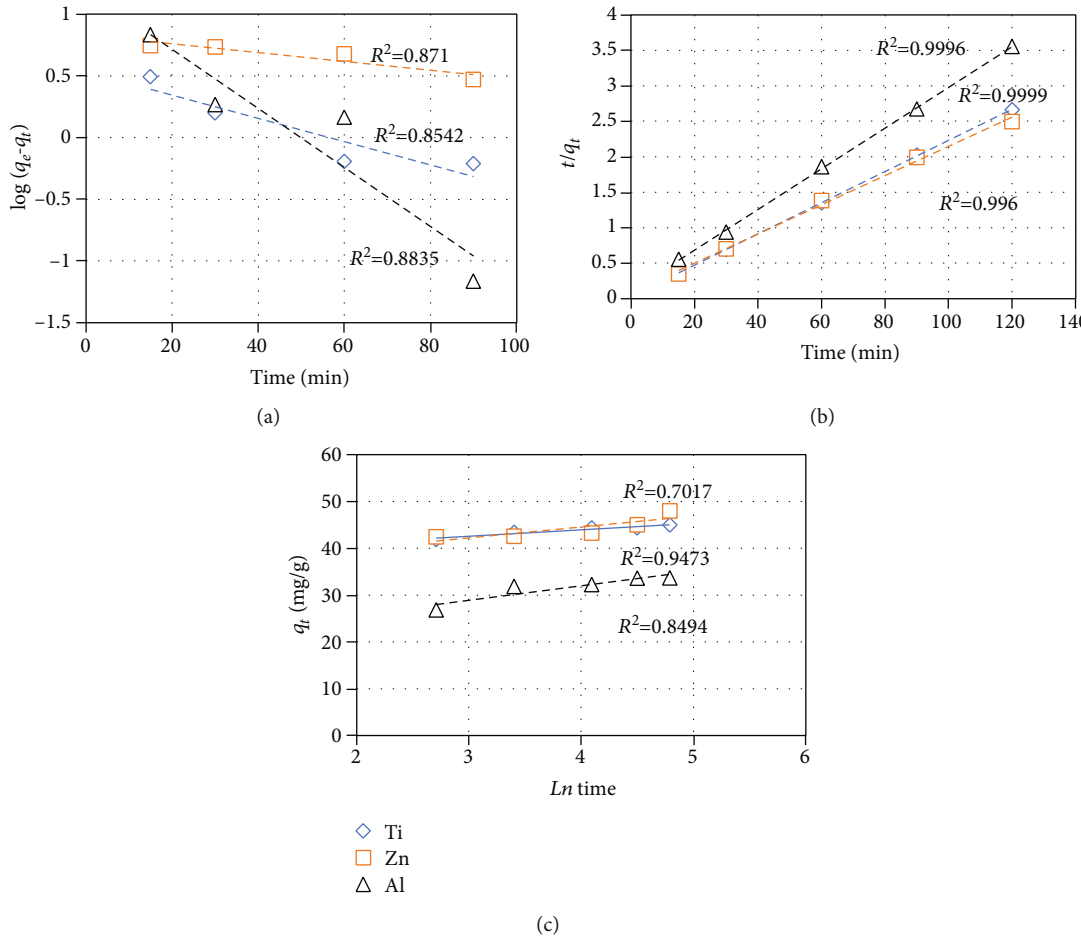

Figure 4: Models for the kinetics of Pb(II) adsorption onto all adsorbents: (a) PFO, (b) PSO, and (c) Elovich's equation.

Table 1: Kinetic parameters for adsorption of Pb(II) onto different adsorbents using PFO, PSO, and Elovich equation.

Kinetic model	Kinetic parameters		ZnO	TiO_2	Al_2O_3
PFO model	k_1	min^{-1}	8.25×10^{-3}	2.17×10^{-2}	5.50×10^{-2}
	$q_{e,cal}$	mg/g	6.79	3.40	15.53
	R^2		0.8710	0.8542	0.8835
PSO model	k_2	g/mg·min	9.3×10^{-4}	1.8×10^{-3}	7.3×10^{-3}
	$q_{e,cal}$	mg/g	48.58	45.37	34.88
	R^2		0.9960	0.9999	0.9996
Elovich equation	a	mg/g·min	9.34×10^{6}	1.03×10^{12}	1.95×10^{3}
	b	g/mg	0.431	0.712	0.327
	R^2		0.7017	0.9473	0.8494

The limiting step of adsorption refers to the slowest step in the process that controls the total adsorption rate. To identify the limiting step of the adsorption mechanism, several kinetic models are commonly used to investigate the rate-limiting step; this included the intraparticle diffusion model as well as the Boyd model. The intraparticle diffusion model was applied to determine the adsorption mechanism. The model is described by Equation (8) [32].

$$q_t = k_{id} * t^{0.5} + C, \tag{8}$$

where q_t is the amount of Pb(II) adsorbed at time t (mg/g), k_{id} is the intraparticle diffusion rate constant (mg/g·$min^{0.5}$), and C is a constant that is related to the thickness of the boundary layer.

Figure 5(a) shows that the plot of Pb(II) uptake against $t^{1/2}$ is not a simple line passing through the origin, indicating

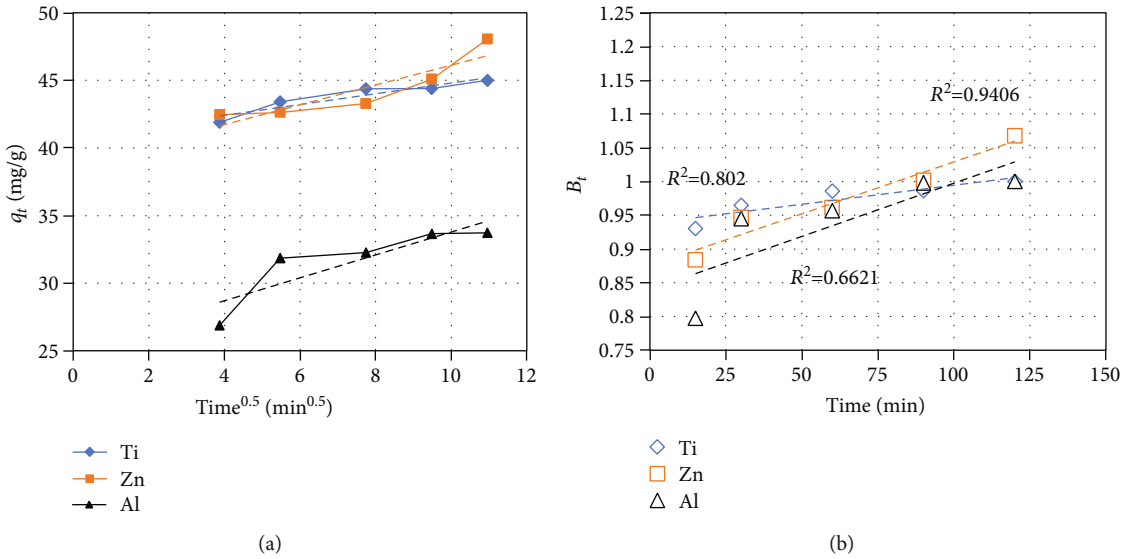

Figure 5: Adsorption mechanisms of Pb(II) onto all adsorbents: (a) intraparticle diffusion model and (b) Boyd kinetic model.

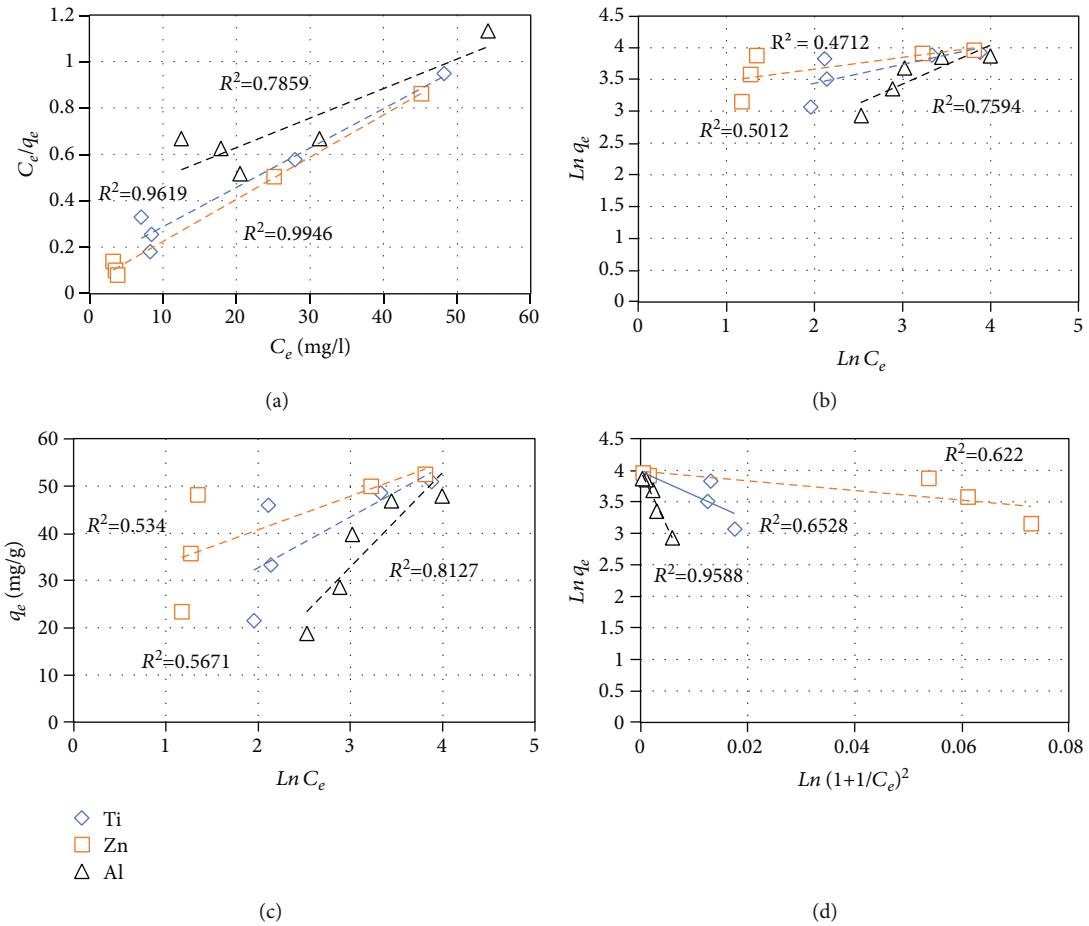

Figure 6: Equilibrium isotherms of Pb(II) onto all adsorbents: (a) Langmuir, (b) Freundlich, (c) Temkin, and (d) Dubinin-Radushkevich.

that the intraparticle diffusion is not the only controlling step limiting the adsorption process. The plot is split into two linear parts for each of the three adsorbents indicating that the adsorption mechanism is a multistep process, where the film diffusion controls the first linear section and the second linear section is controlled by intraparticle diffusion [32–35].

Table 2: Isotherm parameters related to the adsorption of Pb(II) onto adsorbents.

Adsorption isotherms	Isotherm parameters		ZnO	TiO_2	Al_2O_3
Langmuir	q_{max}	mg/g	55.04	58.88	78.49
	a_L	L/mg	0.429	0.144	0.034
	R^2		0.9946	0.9619	0.7859
Freundlich	k_F	mg/g $(mg/L)^{-1/n}$	26.94	17.26	4.91
	n		5.40	3.38	1.63
	R^2		0.4712	0.5012	0.7594
Temkin	B_1	mg/L	7.10	10.78	20.00
	K_T	L/mg	41.80	11.10	0.26
	R^2		0.5340	0.5671	0.8127
Dubinin-Radushkevich	q_D	mg/g	53.96	53.66	53.64
	B	mol^2/J^2	1.22×10^{-6}	6×10^{-6}	2.82×10^{-5}
	R^2		0.6220	0.6528	0.9588

Table 3: Comparison of the adsorption capacities of Pb(II) using various adsorbents.

Material	Adsorption capacity (q_{max}) mg/g	Reference
PDA@rGO/Fe_3O_4	35.2	[9]
Metal-organic framework MIL-100(Fe)	22.864	[1]
Carbon aerogel	0.75	[43]
Zeolite-CuO NCs	45.0	
Zeolite-Fe_3O_4 NCs	50.0	
Nanocomposite of carbon nanotubes/silica	13.0	
Carbon derived from waste rubber	26.0	
ZnO-talc	48.30	
Manganese oxide-coated CNTs	78.74	
TIV	63.29	[44]
Chitosan/magnetite nanocomposite beads	63.3	
4-Aminoantipyrine immobilized bentonite	55.5	
Chitosan crosslinked with epichlorohydrin	34.1	
Pine cone activated carbon	27.53	
Barley straw	23.20	
ZnO	55.04	This research
TiO_2	58.88	
Al_2O_3	53.64	

Furthermore, the Boyd kinetic model is used to determine the slowest step that limits the adsorption process. The model is described by Equation (9) [36], and the results are presented in Figure 5(b).

$$F = \frac{q_t}{q_e} = 1 - \frac{6}{\pi^2} \exp(-Bt). \quad (9)$$

For any adsorbent, a linear plot that succeeds to pass through the origin indicates that the limiting step in the adsorption process is the intraparticle diffusion. However, it is clearly shown in Figure 5(b) that the plot of Bt against time is linear for each of the three adsorbents, but the lines failed to pass through the origin, which indicates that the process is controlled by film diffusion [34, 36].

3.4. Equilibrium Isotherms. Isotherms are the equilibrium relationship between the solid phase and the liquid phase solution concentration. The suitability of a particular adsorbent for extraction of a pollutant can be studied using adsorption isotherms, and the maximum adsorption capacity can also be obtained using various mathematical expressions, such as Langmuir [37], Freundlich [38], Temkin [39],

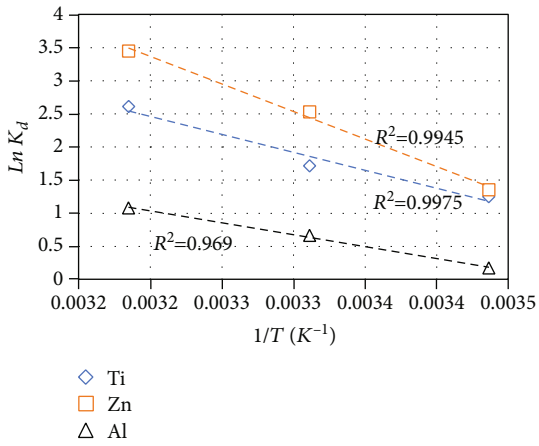

Figure 7: Van't Hoff plot of the adsorption of Pb(II) onto all adsorbents.

Table 4: Thermodynamic parameters for the adsorption of Pb(II) onto all adsorbents.

T (°C)	T (K)	Adsorbent	K_d	$\Delta G°$ (kJ/mol)	$\Delta H°$ (kJ/mol)	$\Delta S°$ (kJ/mol/K)
18	291		3.869	-72.509	69.196	249.409
29	302	ZnO	12.549	-75.252	69.196	249.409
41	314		31.449	-78.245	69.196	249.409
18	291		3.489	-47.764	44.957	164.292
29	302	TiO_2	5.558	-49.571	44.957	164.292
41	314		13.596	-51.543	44.957	164.292
18	291		1.186	-30.435	30.020	104.689
29	302	Al_2O_3	1.939	-31.586	30.020	104.689
41	314		2.943	-32.842	30.020	104.689

and Dubinin-Radushkevich [40] isotherms. These are the most common isotherms used to describe a solid-liquid adsorption system. These isotherms are described by Equation (10), Equation (11), Equation (12), and Equation (13), respectively.

$$\frac{C_e}{q_e} = \frac{1}{K_L} + \frac{a_L}{K_L} C_e, \tag{10}$$

$$\text{Log}\, q_e = \text{Log}\, K_F + \frac{\text{Log}\, C_e}{n}, \tag{11}$$

$$q_e = \frac{RT}{b}\ \ln\,(K_T) + \frac{RT}{b}\ \ln\,(C_e), \tag{12}$$

$$\ln\ q_e = \ln\ q_D - B\varepsilon^2, \tag{13}$$

where K_L is a constant related to the affinity of the binding sites (L/mg), a_L is the Langmuir isotherm, K_F is the Freundlich adsorption constant (mg/g (mg/L)$^{-1/n}$), $1/n$ is the intensity of adsorption in the system, K_T is the constant of equilibrium binding (L/mg), T is the temperature (K), R is the universal gas constant (8.314 J/mol·K), b is the Temkin isotherm constant, C_e is the adsorbate concentration at equilibrium (mg/L), q_D is the theoretical capacity of the adsorbent at saturation (mg/g), B is a constant related to the mean free energy of adsorption per mole of the solute (mol^2/J^2), and ε is the Polanyi potential which is related to equilibrium (kJ^2 mol^2).

Figures 6(a)–6(d) represent plots of the experimental data using the linearized form of the isotherms mentioned above models. Each isotherm has specific assumptions regarding the conditions at which adsorption takes place. Freundlich isothermic adsorption assumes that adsorption occurs on a heterogeneous surface through multilayer adsorption processes, while Langmuir isotherm assumes maximum limiting adsorption at a given number of accessible sites on the adsorbent surface, with the same energy available at all adsorption sites [41, 42]. Temkin isotherm assumes that the adsorption heat decreases linearly as the surface of the adsorbent is covered. The Dubinin-Radushkevich isotherm considers the influence of the porous structure of the adsorbent surface.

The corresponding correlation coefficients (R^2) were determined for each absorbent as shown in Figures 5(a)–5(d). The Langmuir isotherm better described the adsorption behaviour of ZnO and TiO_2, while the adsorption behaviour of Al_2O_3 was best described by the Dubinin-Radushkevich isotherm. Results of equilibrium studies on Pb(II) uptake using ZnO, TiO_2, and Al_2O_3 are summarized in Table 2. Several adsorbents from other studies were compared to the adsorbents used in this research concerning their adsorption capacities, and the comparison is presented in Table 3. According to this comparison, metal oxides have a promising future as an adsorbent in wastewater treatment, as approved by their excellent results.

3.5. Thermodynamics Studies. Since temperature is one of the most important factors in the adsorption processes, the thermodynamics of the adsorption process shall be investigated. To determine the inherent energetic changes that are linked to the adsorption process, thermodynamic constants were investigated by varying the equilibrium constants with temperature to determine: (1) Gibbs free energy ($\Delta G°$), (2) enthalpy ($\Delta H°$), and (3) entropy ($\Delta S°$). The distribution coefficient (K_d) is calculated using Equation (14), followed by Equation (15) [45]:

$$K_d = \frac{q_e}{C_e}, \tag{14}$$

$$\ln K_d = \frac{\Delta S°}{R} - \frac{\Delta H°}{RT}. \tag{15}$$

The values of enthalpy ($\Delta H°$) and entropy ($\Delta S°$) are determined by plotting $\ln K_d$ versus $1/T$ and then calculating the resulting slopes and determining the interception of a Van't Hoff chart as shown in Figure 7. The Gibbs energy ($\Delta G°$) of adsorption is calculated using

$$\Delta G° = \Delta H° - T\Delta S°. \tag{16}$$

The thermodynamic parameters of Pb(II) adsorption onto

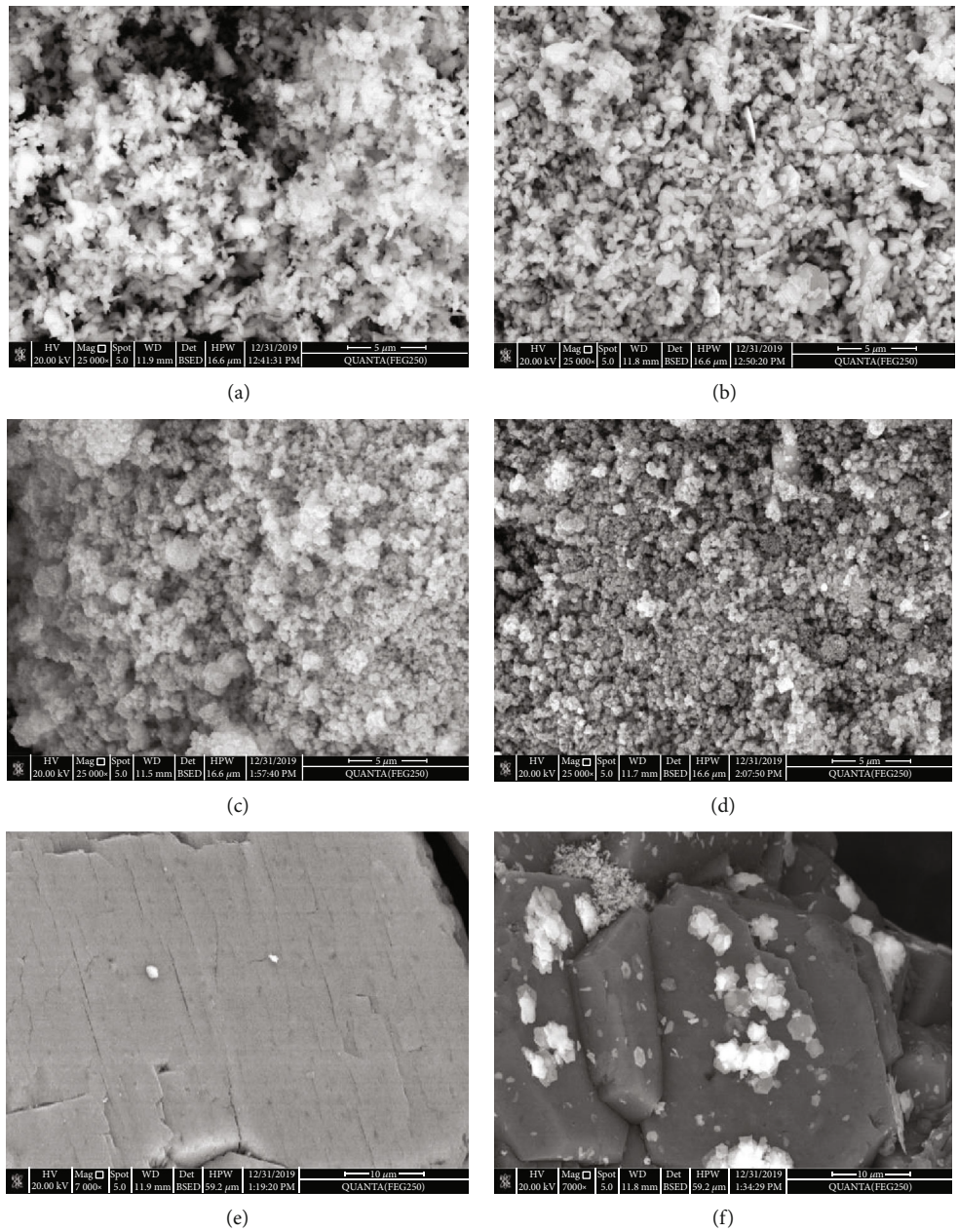

Figure 8: SEM micrograph: (a) unloaded ZnO at 25000x magnification, (b) loaded ZnO at 25000x magnification, (c) unloaded TiO_2 at 25000x magnification, (d) loaded TiO_2 at 25000x magnification, (e) unloaded Al_2O_3 at 7000x magnification, and (f) loaded Al_2O_3 at 7000x magnification.

ZnO, TiO_2, and Al_2O_3 are summarized in Table 4. The positive enthalpy values indicate that Pb(II) adsorption by ZnO, TiO_2, and Al_2O_3 is an endothermic process. In addition, the high enthalpy values ($\Delta H^\circ > 20$ kJ/mol) indicate that chemisorption is involved in the adsorption process as an ion exchange mechanism [46]. The positive values for entropy reflect excess randomness at the solid-liquid interface through the adsorption process. The negative values of the Gibbs energy indicate that the procedure is spontaneous and that this spontaneity increases as the temperature increases.

3.6. The Morphological and Chemical Composition of the Adsorbents. The morphology of the adsorbents' surface was examined using the SEM test, where SEM images revealed changes in the morphology of the adsorbents before and after the adsorption process, see Figures 8(a)–8(f). The SEM images (Figures 8(a) and 8(c)) showed that both ZnO and TiO_2 exhibit tough and irregular surfaces with spongy openings before the adsorption process. In contrast, the SEM images for Al_2O_3, Figures 8(e), show solid and smooth surfaces with few porous openings. This may explain the low removal efficiency of Pb(II) using Al_2O_3 compared to ZnO and TiO_2. After the adsorption process (Figures 8(b), 8(d), and 8(f)), the porous openings on ZnO, TiO_2, and Al_2O_3 surfaces were filled. The comparison of the SEM images of ZnO, TiO_2, and Al_2O_3 before and after Pb(II) uptake at

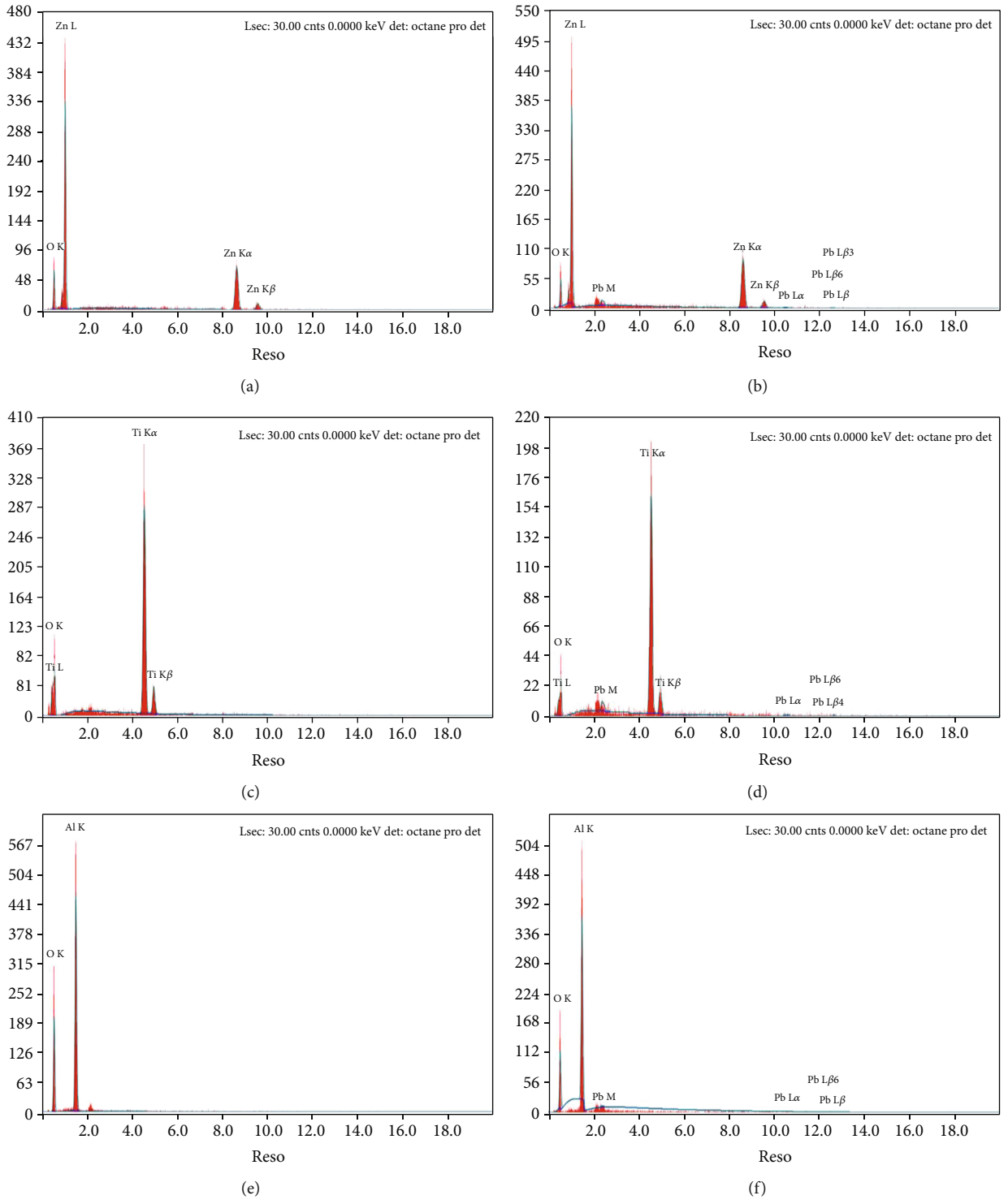

Figure 9: EDX pattern: (a) unloaded ZnO, (b) loaded ZnO, (c) unloaded TiO_2, (d) loaded TiO_2, (e) unloaded Al_2O_3, and (f) loaded Al_2O_3.

different magnification scales reveals a clear change in the morphology and emphasizes that adsorption occurred.

EDX analysis was used to determine the elemental and chemical composition of a sample and measure the amount of trace elements. EDX analysis provided further affirmation of Pb(II) uptake on ZnO, TiO_2, and Al_2O_3. Figures 9(a)–9(f) show the EDX spectra for ZnO, TiO_2, and Al_2O_3 before (unloaded) and after (loaded) the adsorption process. Figures 9(a), 9(c), and 9(e) show no characteristic signals for any metal ions except for Zn^{2+}, Ti^{2+}, and Al^{3+}, respectively. On the other hand, Pb(II) signals were observed in Figures 9(b), 9(d), and 9(f). This shows the accumulation of Pb(II) onto the surface of ZnO, TiO_2, and Al_2O_3 particles.

4. Conclusions

In this research, a comprehensive study of lead removal by adsorption was conducted using three different metal oxide adsorbents, namely, zinc oxide (ZnO), titanium dioxide (TiO_2), and aluminium oxide (Al_2O_3). The points of zero charge for the considered adsorbents were found to be 7.3, 7.1, and 9.0 for ZnO, TiO_2, and Al_2O_3, respectively. The effect of pH of the solution, adsorbent dose, contact time, initial concentrations, and temperature on the adsorption process and removal efficiency was studied. The optimal values of these parameters were obtained using separate batch experiments. After applying the optimal values of the studied adsorption parameters for the adsorbents, the adsorption kinetics were investigated using different models, such as PFO, PSO, and Elovich equation, where PSO best fit the adsorption of lead for all of the adsorbents.

Furthermore, the adsorption mechanism was investigated using the intraparticle adsorption and Boyd kinetic models. The intraparticle adsorption model showed that the adsorption of lead was a multistep controlled mechanism, while Boyd's kinetic model showed that the film diffusion mechanism is the limiting step of the adsorption process for all the considered adsorbents. In addition, the adsorption isotherms were studied at equilibrium. The results showed that the Langmuir isotherm model best described the adsorption of lead by ZnO and TiO_2, while the adsorption behaviour of Al_2O_3 was best fitted by the Dubinin-Radushkevich isotherm model. The thermodynamic studies showed that the adsorption of lead onto ZnO, TiO_2, and Al_2O_3 was endothermic and spontaneous. Finally, the morphological and chemical compositions of the adsorbents were tested using SEM and EDX analysis. The SEM images showed that both ZnO and TiO_2 surfaces had very porous holes compared to Al_2O_3. Changes in the adsorbent morphologies confirmed that adsorption occurred. The EDX spectra illustrated the presence of lead signals after the adsorption process, ensuring that lead ions had accumulated onto the surface of the ZnO, TiO_2, and Al_2O_3 particles. At the end, it can be concluded that under the optimal conditions adopted in this study, lead removal from aqueous solutions by adsorption is best obtained using ZnO followed by TiO_2 and finally comes Al_2O_3.

Data Availability

The authors confirm that the data supporting the findings of this study are available within the article.

Conflicts of Interest

The authors declare that they have no conflicts of interest.

References

[1] M. Forghani, A. Azizi, M. J. Livani, and L. A. Kafshgari, "Adsorption of lead(II) and chromium(VI) from aqueous environment onto metal- organic framework MIL-100(Fe): Synthesis, kinetics, equilibrium and thermodynamics," *Journal of Solid State Chemistry*, vol. 291, 2020.

[2] S. V. Mousavi, A. Bozorgian, N. Mokhtari, M. A. Gabris, H. R. Nodeh, and W. A. Ibrahim, "A novel cyanopropylsilane-functionalized titanium oxide magnetic nanoparticle for the adsorption of nickel and lead ions from industrial wastewater: equilibrium, kinetic and thermodynamic studies," *Microchemical Journal*, vol. 145, pp. 914–920, 2019.

[3] A. Elawwad, A. Naguib, and H. Abdel-Halim, "Modeling of phenol and cyanide removal in a full-scale coke-oven wastewater treatment plant," *Desalination and Water Treatment*, vol. 57, no. 52, pp. 25181–25193, 2016.

[4] A.-K. F. A. Ihsanullah, F. A. al-Khaldi, B. Abusharkh et al., "Adsorptive removal of cadmium(II) ions from liquid phase using acid modified carbon-based adsorbents," *Journal of Molecular Liquids*, vol. 204, pp. 255–263, 2015.

[5] M. Bilal, I. Ihsanullah, M. Younas, and M. Ul Hassan Shah, "Recent advances in applications of low-cost adsorbents for the removal of heavy metals from water: a critical review," *Separation and Purification Technology*, vol. 278, 2021.

[6] M. K. Uddin, "A review on the adsorption of heavy metals by clay minerals, with special focus on the past decade," *Chemical Engineering Journal*, vol. 308, pp. 438–462, 2017.

[7] F. Ge, M. M. Li, H. Ye, and B. X. Zhao, "Effective removal of heavy metal ions Cd^{2+}, Zn^{2+}, Pb^{2+}, Cu^{2+} from aqueous solution by polymer-modified magnetic nanoparticles," *Journal of Hazardous Materials*, vol. 211-212, pp. 366–372, 2012.

[8] M. Ghorbani, O. Seyedin, and M. Aghamohammadhassan, "Adsorptive removal of lead (II) ion from water and wastewater media using carbon-based nanomaterials as unique sorbents: A review," *Journal of Environmental Management*, vol. 254, 2020.

[9] A. Mehdinia, S. Heydari, and A. Jabbari, "Synthesis and characterization of reduced graphene oxide- Fe_3O_4@polydopamine and application for adsorption of lead ions: Isotherm and kinetic studies," *Materials Chemistry and Physics*, vol. 239, article 121964, 2020.

[10] H. Yang, M. Lu, D. Chen, R. Chen, L. Li, and W. Han, "Efficient and rapid removal of Pb^{2+} from water by magnetic Fe_3O_4@MnO_2 core-shell nanoflower attached to carbon microtube: adsorption behavior and process study," *Journal of Colloid and Interface Science*, vol. 563, pp. 218–228, 2020.

[11] Y. Zhang, X. Song, P. Zhang, H. Gao, C. Ou, and X. Kong, "Production of activated carbons from four wastes via one-step activation and their applications in Pb^{2+} adsorption: insight of ash content," *Chemosphere*, vol. 245, 2020.

[12] M. El Ouardi, M. Laabd, H. Abou Oualid et al., "Efficient removal of p-nitrophenol from water using montmorillonite clay: insights into the adsorption mechanism, process optimization, and regeneration," *Environmental Science and Pollution Research*, vol. 26, pp. 19615–19631, 2019.

[13] P. M. Thabede, N. D. Shooto, and E. B. Naidoo, "Removal of methylene blue dye and lead ions from aqueous solution using activated carbon from black cumin seeds," *South African Journal of Chemical Engineering*, vol. 33, pp. 39–50, 2020.

[14] V. Novoseltseva, H. Yankovych, O. Kovalenko, M. Václavíková, and I. Melnyk, "Production of high-performance lead(II) ions adsorbents from pea peels waste as a sustainable resource," *Waste Management & Research*, vol. 39, no. 4, pp. 584–593, 2021.

[15] R. Arora, "Adsorption of heavy metals-a review," *Materials Today: Proceedings*, vol. 18, pp. 4745–4750, 2019.

[16] M. Gu, L. Hao, Y. Wang et al., "The selective heavy metal ions adsorption of zinc oxide nanoparticles from dental wastewater," *Chemical Physics*, vol. 534, 2020.

[17] A. H. Saad, A. M. Azzam, S. T. El-Wakeel, B. B. Mostafa, and M. B. Abd El-latif, "Removal of toxic metal ions from wastewater using ZnO@Chitosan core-shell nanocomposite," *Environmental Nanotechnology, Monitoring & Management*, vol. 9, pp. 67–75, 2018.

[18] Z. Wu, X. Liu, C. Yu, F. Li, W. Zhou, and L. Wei, "Construct interesting CuS/TiO_2 architectures for effective removal of Cr(VI) in simulated wastewater *via* the strong synergistic adsorption and photocatalytic process," *Science of The Total Environment*, vol. 796, 2021.

[19] S. Tabesh, F. Davar, and M. R. Loghman-Estarki, "Preparation of γ-Al_2O_3 nanoparticles using modified sol-gel method and its use for the adsorption of lead and cadmium ions," *Journal of Alloys and Compounds*, vol. 730, pp. 441–449, 2018.

[20] A. Herrera-Barros, C. Tejada-Tovar, A. Villabona-Ortíz, Á. González-Delgado, and R. J. Mejía-Meza, "Assessment of the effect of Al_2O_3 and TiO_2 nanoparticles on orange peel biomass and its application for Cd(II) and Ni(II) uptake," *Transactions of the ASABE*, vol. 62, no. 1, pp. 139–147, 2019.

[21] A. Herrera-Barros, C. Tejada-Tovar, A. Villabona-Ortíz, A. D. González-Delgado, and J. Benitez-Monroy, "Cd (II) and Ni (II) uptake by novel biosorbent prepared from oil palm residual biomass and Al_2O_3 nanoparticles," *Sustainable Chemistry and Pharmacy*, vol. 15, 2020.

[22] A. Herrera, C. Tejada-Tovar, and Á. D. González-Delgado, "Enhancement of cadmium adsorption capacities of agricultural residues and industrial fruit byproducts by the incorporation of Al2O3Nanoparticles," *ACS Omega*, vol. 5, no. 37, pp. 23645–23653, 2020.

[23] Y. S. Al-Degs, M. I. El-Barghouthi, A. H. El-Sheikh, and G. Walker, "Effect of solution pH, ionic strength, and temperature on adsorption behavior of reactive dyes on activated carbon," *Dyes and Pigments*, vol. 77, no. 1, pp. 16–23, 2008.

[24] P. C. C. Faria, J. J. M. Órfão, and M. F. R. Pereira, "Adsorption of anionic and cationic dyes on activated carbons with different surface chemistries," *Water Research*, vol. 38, pp. 2043–2052, 2004.

[25] EPA, *Methods for determination of metals in environmental samples*, Office of Research and Development, Washington DC, 1991.

[26] D. O. Cooney, *Adsorption Design for Wastewater Treatment |Open Library*, Lewis Publisher, 1999.

[27] V. C. Taty-Costodes, H. Fauduet, C. Porte, and A. Delacroix, "Removal of Cu(II) and Pb(II) ions from aqueous solutions by adsorption on sawdust of Meranti wood," *Desalination*, vol. 247, pp. 636–646, 2009.

[28] G. Blanchard, M. Maunaye, and G. Martin, "Removal of heavy metals from waters by means of natural zeolites," *Water Research*, vol. 18, pp. 1501–1507, 1984.

[29] S. Lagergren, "About the theory of so-called adsorption of soluble substances," *Sven Vetenskapsakad Handingarl*, vol. 24, pp. 1–39, 1898.

[30] I. S. McLintock, "The elovich equation in chemisorption kinetics," *Nature*, vol. 216, no. 5121, pp. 1204-1205, 1967.

[31] P. Senthil Kumar, S. Ramalingam, R. V. Abhinaya, S. D. Kirupha, T. Vidhyadevi, and S. Sivanesan, "Adsorption equilibrium, thermodynamics, kinetics, mechanism and process design of zinc(II) ions onto cashew nut shell," *The Canadian Journal of Chemical Engineering*, vol. 90, pp. 973–982, 2012.

[32] W. J. Weber and J. C. Morris, "Kinetics of adsorption on carbon from solution," *Journal of the Sanitary Engineering Division*, vol. 89, no. 2, pp. 31–59, 1963.

[33] P. Senthil Kumar, C. Senthamarai, and A. Durgadevi, "Adsorption kinetics, mechanism, isotherm, and thermodynamic analysis of copper ions onto the surface modified agricultural waste," *Environmental Progress & Sustainable Energy*, vol. 33, no. 1, pp. 28–37, 2014.

[34] D. Balarak, M. Zafariyan, C. A. Igwegbe, K. K. Onyechi, and J. O. Ighalo, "Adsorption of acid blue 92 dye from aqueous solutions by single-walled carbon nanotubes: isothermal, kinetic, and thermodynamic studies," *Environmental Processes*, vol. 8, no. 2, pp. 869–888, 2021.

[35] D. Balarak, T. J. al-Musawi, I. A. Mohammed, and H. Abasizadeh, "The eradication of reactive black 5 dye liquid wastes using Azolla filiculoides aquatic fern as a good and an economical biosorption agent," *SN Applied Sciences*, vol. 2, no. 6, 2020.

[36] G. E. Boyd, A. W. Adamson, and L. S. Myers, "The exchange adsorption of ions from aqueous solutions by organic zeolites. II. Kinetics1," *Journal of the American Chemical Society*, vol. 69, no. 11, pp. 2836–2848, 1947.

[37] I. Langmuir, "The adsorption of gases on plane surfaces of glass, mica and platinum," *Journal of the American Chemical Society*, vol. 40, pp. 1361–1403, 1918.

[38] H. Freundlich, "Über die adsorption in lösungen," *Zeitschrift für Physikalische Chemie*, vol. 57U, pp. 385–470, 1907.

[39] M. J. Temkin and V. Pyzhev, "Recent modifications to Langmuir isotherms," *Acta Physiochim URSS*, vol. 12, pp. 217–222, 1940.

[40] M. M. Dubinin and L. V. Radushkevich, "Equation of the characteristic curve of activated charcoal," in *Proceedings of the Academy of Sciences, Physical Chemistry Section USSR*, pp. 331–333, New York, 1947.

[41] V. Fierro, V. Torné-Fernández, D. Montané, and A. Celzard, "Adsorption of phenol onto activated carbons having different textural and surface properties," *Microporous and Mesoporous Materials*, vol. 111, pp. 276–284, 2008.

[42] H. N. Tran, S. J. You, A. Hosseini-Bandegharaei, and H. P. Chao, "Mistakes and inconsistencies regarding adsorption of contaminants from aqueous solutions: a critical review," *Water Research*, vol. 120, pp. 88–116, 2017.

[43] H. A. Sani, M. B. Ahmad, and T. A. Saleh, "Synthesis of zinc oxide/talc nanocomposite for enhanced lead adsorption from aqueous solutions," *RSC Advances*, vol. 6, pp. 108819–108827, 2016.

[44] M. Naushad, Z. A. ALOthman, M. R. Awual, M. M. Alam, and G. E. Eldesoky, "Adsorption kinetics, isotherms, and thermodynamic studies for the adsorption of Pb2+ and Hg2+ metal ions from aqueous medium using Ti(IV) iodovanadate cation exchanger," *Ionics*, vol. 21, no. 8, pp. 2237–2245, 2015.

[45] X. Zhao, Q. Jia, N. Song, W. Zhou, and Y. Li, "Adsorption of Pb(II) from an aqueous solution by titanium dioxide/carbon nanotube nanocomposites: kinetics, thermodynamics, and isotherms," *Journal of Chemical and Engineering Data*, vol. 55, no. 10, pp. 4428–4433, 2010.

[46] L. J. Kennedy, J. J. Vijaya, G. Sekaran, and K. Kayalvizhi, "Equilibrium, kinetic and thermodynamic studies on the adsorption of m-cresol onto micro- and mesoporous carbon," *Journal of Hazardous Materials*, vol. 149, pp. 134–143, 2007.